Proceedings of the 20th International Conference on Soil Mechanics and Geotechnical Engineering– Rahman and Jaksa (Eds)

Multi-scale geo-mechanics on scour

Géomécanique multi-échelle sur affouillement

Kaiga Yasue & Kenichi Maeda
Department of Civil Engineering, Nagoya Institute of Technology, Japan, k.yasue.493@stn.nitech.ac.jp

Tatsuya Matsuda
Department of Civil Engineering, Toyohashi University of Technology, Japan

ABSTRACT: In studies on the scouring phenomenon, tractive force has been widely used for evaluation. Evaluation by tractive force is done from a microscopic viewpoint, focusing on the balance between the shear force generated by the fluid on the ground surface and the effective weight of a soil particle in the outermost ground layer. However, when we consider the scouring phenomena that occurs around structures and on account of overtopping, the scale of scouring is such that it cannot be explained merely from the viewpoint of tractive force. Moreover, it has been pointed out in recent studies that the effect of fluid force does not only to affect the ground surface, but also causes stress changes inside the ground, thereby promoting scouring. Therefore, besides the microscopic view, it is necessary to elucidate the phenomena regarding the meso-scale of soil elements and to consider a wide range of perspectives of the macro scale of structures. Therefore, this paper demonstrates some of the findings from our research on the scour phenomenon focusing on soil-fluid interaction in multiple scales.

RÉSUMÉ : Dans les études sur le phénomène d'affouillement, la force de traction a été largement utilisée pour l'évaluation. L'évaluation par force de traction se fait d'un point de vue microscopique, en se concentrant sur l'équilibre entre la force de cisaillement générée par le fluide à la surface du sol et le poids effectif d'une particule de sol dans la couche la plus externe du sol. Cependant, lorsque l'on considère les phénomènes d'affouillement qui se produisent autour des ouvrages et du fait du franchissement, l'ampleur de l'affouillement est telle qu'elle ne peut s'expliquer du seul point de vue de la force de traction. De plus, il a été souligné dans des études récentes que l'effet de la force du fluide n'affecte pas seulement la surface du sol, mais provoque également des changements de contraintes à l'intérieur du sol, favorisant ainsi l'affouillement. Par conséquent, outre la vue microscopique, il est nécessaire d'élucider les phénomènes concernant la méso-échelle des éléments du sol et d'envisager un large éventail de perspectives de la macro-échelle des structures. Par conséquent, cet article démontre certains des résultats de nos recherches sur le phénomène d'affouillement en se concentrant sur l'interaction sol-fluide à plusieurs échelles.

KEYWORDS: Scouring; Seepage; Excess pore water pressure; Micromechanics; Destabilization.

1 INTRODUCTION

1.1 *Damage to waterfront facilities with scouring*

Scouring of the ground caused by tsunami currents cause large-scale topographical changes and decrease the bearing capacity of structures, causing enormous amounts of damage. During the Great East Japan Earthquake that occurred in 2011, the scouring of the ground near coastal structures weakened structures and removed their wave-resistant function, causing and spreading damage (Matsuda, et al., 2016) [1]. With regard to increasing or sustained high water levels due to floods caused by frequent heavy rains, crisis management measures that minimize damage from scouring caused by riverbed fluctuations, river embankment piping destruction, erosion breakdown, and overflow destruction are an urgent issue.

1.2 *Multi-scale dynamics*

Research focusing on the scouring phenomenon has conventionally involved the active evaluation of tractive force and predictions of topographical changes due to the water flow. The prediction method is evaluated from a microscopic viewpoint, which focuses on the equilibrium conditions between the shearing force generated by the fluid force and the effective weight of soil particles on the outermost layer of the ground. However, the scouring phenomenon of waterfront structures cannot be explained only from the perspective of tractive force when considering the scale of occurrence. Recent studies have considered how the fluid force not only affects the ground surface layer but also generates changes in stress inside the ground and promotes scouring (Suzuki, et al., 2016; Matsuda et al., 2016).

2 CRITICAL FLOW VELOCITIES FOR SOILS

The method of understanding the scouring problem varies depending on the position of the research field. Hydraulics, which focuses on the flow of water, studies the modeling of bottom topography and surface particle behaviors. Conversely, ground mechanics focuses on the deformation/fracture behavior of soil elements by varying the effective stress due to the contact force between particles propagating in the soil particle skeleton. Therefore, the former can be considered the "fish" perspective, whereas the latter is the "clam" perspective. The third perspective on granular materials connects the two perspectives and involves liquefaction and fluidization of soil elements due to variations in effective stress caused by the seepage of water on the ground surface layer.

Figure 1 summarizes the flow velocities acting on soil and soil structures and provides an overview of the velocity domains of the seepage of water passing through the soil interior and the velocity at which phenomena, such as quicksand and erosion due to surface flows, occur (the relationship between the characteristic flow velocity and grain size D is arranged). For comparison, rainfall that causes soil infiltration is depicted by converting the hourly rainfall mm/*hr*, which is the rainfall intensity, to the dimensions of velocity mm/*s*. The Creager's

equation on hydraulic conductivity k (units of velocity) when Darcy's law holds for the seepage flow; the critical velocity v_{crit} calculated from the Reynold's number R_e (v is the apparent flow velocity, D is the average particle size, ρ_w is the water density, μ is the viscosity coefficient, and υ is the kinematic viscosity coefficient $\upsilon = \mu/\rho_w$); the Justin critical flow velocity v_j for a single particle lift-off; Rubey's equation w_f for a single particle's settling speed; and the critical friction velocity u_{*c} (Iwagaki's formula) where the critical tractive force (shear stress), which controls the quicksand phenomenon, is expressed in units of flow velocity are shown in the figure. $u_{*c} > w_f$ when D is approximately 0.1 mm or less, whereas $u_{*c} < w_f$ when D is 0.1 mm or more. Consequently, the characteristics of the quicksand behavior change.

Furthermore, the ratios of v_j, w_f, and u_{*c} relative to the hydraulic conductivity k are approximately 1300, 500, and 750, respectively, when D = 0.1 mm. These values are 100 or less when D = 0.5 mm, and they become smaller as D increases. The following conditions are needed for water to seep into the solid-phase soil mass and a transition with intense movements such as that of quicksand from a state with immobile soil particles: ① layers with different contact permeabilities are in contact, and ② flow is three-dimensionally localized and concentrated and the solid phase is transitioning to the liquid phase. When fast flows are acting on the ground surface, the flow velocity widely varies between the inside and outside of the ground with the ground surface as the boundary, and this phenomenon tends to become discontinuous. However, the seepage flow into the soil is also generated, and the pressure gradient of pore water, local flow deformation, and unstable infiltration may all be induced at the boundary.

In this article, we report the results of an extremely simple model experiment and theoretical consideration as an attempt to elucidate the relationship between the scouring and seepage phenomena from a wide range of multi-scale perspectives, not just from a particle-level microscale or structural-level macroscale perspective but also from the soil element-level perspective (mesozone scale).

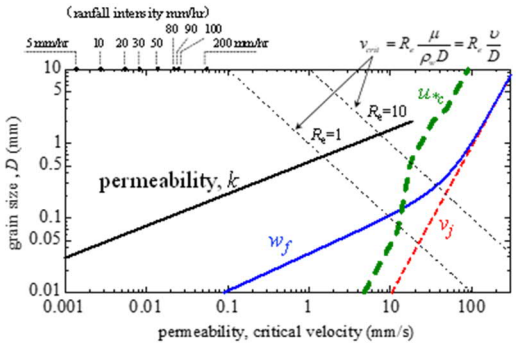

Figure 1. Critical flow velocities with soil grain sizes.

3 SCOURING MECHANISMS BY AN OPEN CHANNEL FLOW

3.1 *Overview of the experimental method*

A test apparatus of 2.0 m × 0.3 m × 0.3 m (length, width, height) acrylic open channel with a mobile seabed was used as the experimental equipment shown in Figure 2). A test apparatus of 0.5 m × 0.3 m × 0.1 m (length, width, height) mobile seabed section of the open channel was set up. The pump was used to generate the circulating flow of the water. Toyoura sand (average particle size D_{50} = 0.17 mm) with different relative density D_r conditions (loose packing: D_r = 40%, dense packing: D_r = 70%) was controlled to be under saturated conditions to analyze the scouring phenomena in detail. The soil particle size was predominant in common findings relating to conventional scouring, and density has not been considered important. However, for this experiment, we measured the cross-sectional flow velocity distributions of the fluid using a pitot tube and measurements of the pore water pressure in the ground using small pore water pressure sensors (resolution: 5 Pa). The installation locations of the pore water pressure sensors within the mobile seabed are shown in the figure. Imaging was also performed using a high-speed camera and a video camera. It can be confirmed from the captured images that the movements, which could be observed at the wall surface even in the depth direction, occur in a relatively uniform manner.

The Prandtl–von Kármán logarithmic distribution law was used to determine the friction velocity u^* on the surface of the sedimentary layer and calculate the dimensionless tractive force τ^*. The dimensionless tractive force was τ^* = 0.129 in the Toyoura sand, exceeding the dimensionless critical tractive force τ_c^* = 0.075, which used the friction velocity on the mobile seabed. This finding is theoretically a condition under which scouring would occur, and given that scouring has actually occurred, the validity of the prediction equation has been confirmed.

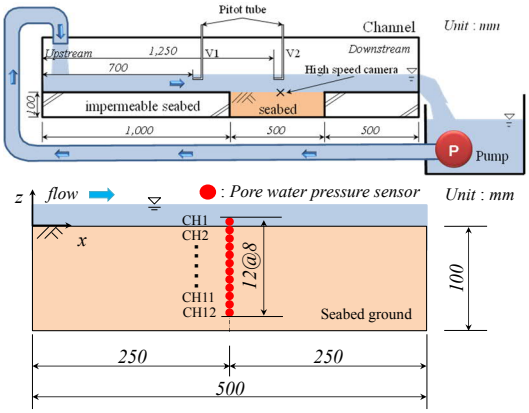

Figure 2. Experiment apparatus for the open channel.

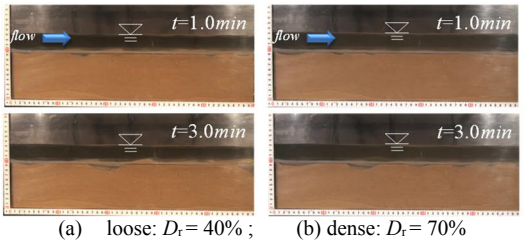

(a) loose: D_r = 40% ; (b) dense: D_r = 70%

Figure 3. Experiment apparatus for the open channel.

3.2 *Overall observational results of scouring*

3.2.1 *Dune formation and scouring/erosion rate*

The scouring behavior during the experiments is shown in Fig. 3. Scouring occurred on the ground surface layer, and the repeated movement and deposition of the soil particles resulted in the formation of riverbed waves referred to as dunes. Moreover, flow deformation in the downstream direction was observed. Therefore, comparisons of the dune flow-down velocities according to differences in the relative density of the ground showed that the loosely packed ground with D_r = 40% more rapidly formed dunes, and the velocity of flow deformation was

also larger (Figure 4). There were not many differences in the final scouring amount.

To date, several formulas have been proposed for scouring and erosion velocities based on experimental results. For example, Wang and Bowles targeted the embankment erosion of non-adhesive sandy soil and gravel and expressed the scouring/erosion rate E with tractive force τ and critical tractive force τ_c. Sandy soil was also used in this experiment, so the scouring/erosion velocity (60 s after the start of experiments) was estimated from the above equation, as shown in Figure 5, together with the experimental measurement values (equation is shown in the figure). E is independent of the soil element density in the estimation equation. However, although E is relatively close to the estimation equation in the dense ground of $D_r = 70\%$, E is approximately six times larger than the dense ground in the case of the loose ground of $D_r = 40\%$, diverging considerably from the estimation equation and showing that the scouring rate was caused by the density of the ground.

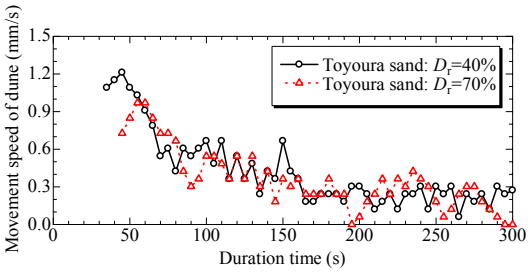

Figure 4. Flow- down velocity of sand wave on bed.

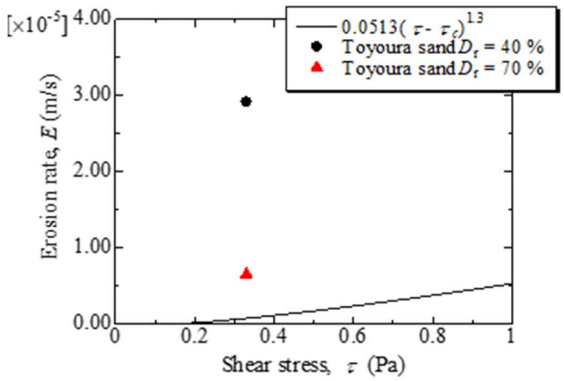

Figure 5. Scour rates with different sand mass densities.

3.2.2 *Calculation example of pore water pressure changes in the ground*

The variable excess water pressure was calculated by subtracting the hydrostatic pressure from the measured pore water pressure. The excess pore water pressure ratio u_e/σ'_0, which is the ratio of the variable excess pore water pressure to the initial effective overburden pressure σ'_0, was calculated; the distribution in the depth direction z is shown in Figure 6. The excess pore water pressure ratio indicates that a liquefaction state is reached when the value is 1.0, and considerable decreases in the bearing capacity of the ground are assumed to happen when the value is 0.5 or above. The excess pore water pressure ratio reached 1.0 in the surface layer for the loose ground (D_r = 40%), and a state similar to that of liquefaction was reached. Similarly, excess pore water pressure ratios of 0.5 or over were reached at depths z = −7.75 mm or shallower from the surface layer. Meanwhile, the excess pore water pressure ratio in the surface layer was approximately 0.6, even for the dense ground (D_r = 70%), and excess pore water pressure ratios of 0.5 or over were reached at depths of z = −4.60 mm or shallower from the surface layer. In other words, excess pore water pressure was generated in the ground surface layer in either case, so a flow with an upward component was generated toward the ground surface at the outermost layer. However, the water balance in these cases does not match, hence forming a contradiction.

Furthermore, details are omitted due to space limitations, but we attempted to calculate the excess pore water pressure ratio distribution based on simple theoretical solutions. The formation of pressure difference due to velocity differences in the upper and lower sections of particles in the ground surface layer can explain the increase in excess pore water pressure at the outermost layer of the ground, but it cannot explain the increases at depths found in these experimental results. The existence of a fluidized bed due to the movement of particles within a given layer thickness of the surface layer, dilatancy deformations, and the movement of pore water to a given depth needs to be confirmed. Therefore, the movement of soil particles and pore water was observed.

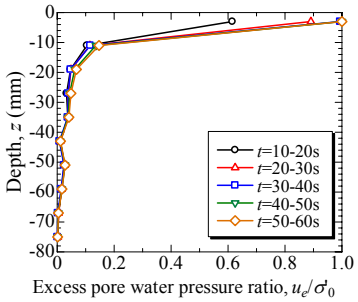

(a) Loose sand: D_r = 40%

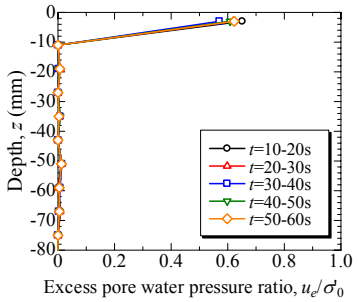

(b) Dense sand: D_r = 70%

Figure 6. Excess pore water pressure ratio in sands.

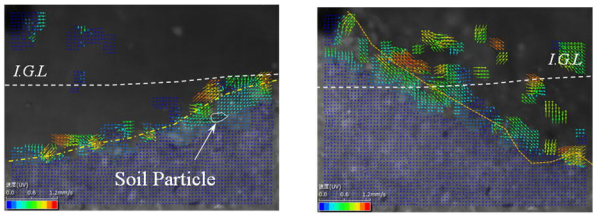

(a) In the back of the ripple (b) In the front of the ripple

Figure 7. Sand particle velocities around the sand ripple.

3.3 *Observation of soil particles and movement phenomena of soil particle groups*

Figure 7 shows the particle-level movements around the sand slab. Complicated changes in the flow around the sand slab caused the soil particles to move, lift, and flow in the direction opposite to the flow down direction on the back surface of the sand slab upstream of the flow. Some of these particles were also

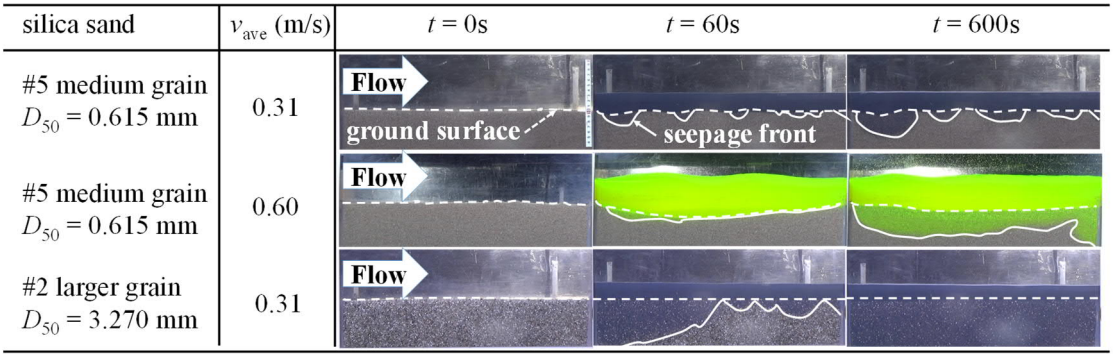

Figure 8. Seepage behaviors in grounds with different flow velocities by observation method (A).

washed away to the front of the sand slab on the downstream side, whereas some were moved via convection. The deposition of the soil particles that moved from the back surface of the sand slab was observed in the front of the sand slab in the downstream direction. Furthermore, the surface layer collapsed from the sand slope to a maximum depth of approximately 1 mm (approximately seven soil particles' worth), which seemed to prompt the movement of the sand slab itself. Ultimately, the existence of a clear fluidized bed and the confirmation of the layer that deforms the dilatancy has not been clearly confirmed at this time.

3.4 *Observation of seepage into the ground surface layer*

3.4.1 *Experimental methods and seepage observation*

The Toyoura sand used in the previous experiment had a small particle size (average particle size D_{50} = 0.173 mm), and the observation of the seepage behavior was thought to be difficult. Therefore, silica sand No. 5 (#5, D_{50} = 0.615 mm) and No. 2 (#2, D_{50} = 3.270 mm), which have relatively uniform and large particle sizes, were used. The relative density was set to D_r = 40%. A submersible pump (average cross-sectional flow velocity: 0.31 m/s, 0.60 m/s) was used to generate the circulating water flow.

We attempted to observe seepage through three observation methods: (A) dying the circulating fluid beforehand with either black ink or fluorescent-colored uranine solution; (B) directly injecting uranine solution into the ground surface with a syringe and observing its movement alongside the flow; and (C) injecting the uranine solution in advance into the ground in a vertical columnar shape and where the pore water movement in the ground when the flow is activated is observed with the column deformation.

3.4.2 *Observation results and discussion*

Figure 8 shows the seepage of the horizontal flow fluid into the ground using the seepage observation method (A). Partial seepage occurred, and ripples were formed in the ground. The wavelength of the ripple region was longer when the average cross-sectional flow velocity v_{ave} in the open channel was large (0.60 m/s). The wavelength became longer when silica sand No. 2 was used, which had a large particle size and for which no riverbed waves were formed.

The variable excess water pressure was calculated by subtracting the hydrostatic pressure from the measured pore water pressure. The excess pore water pressure ratio u_e/σ'_0, which is the ratio of Observing seepage with seepage observation method (B) in Figure 9, inflows into the ground can be seen from the valleys scoured on the sand slab, with seepage occurring along the arcs of the peaks and larger arcs forming as the valleys were deeper. In other words, the ripple seepage was formed by parallel arc-shaped seepage trajectories of different sizes, and the size of the riverbed wave was thought to have a large influence on the arc size.

Figure 10 shows that when using seepage observation method (C), the pore water in the ground moved in a large arc to the depths due to seepage from the surface, as described above. No details of the flow near the surface layer can be observed. Accordingly, arc-like seepage trajectories appears to form, and the size of these arcs increased in the depth direction from the ground surface.

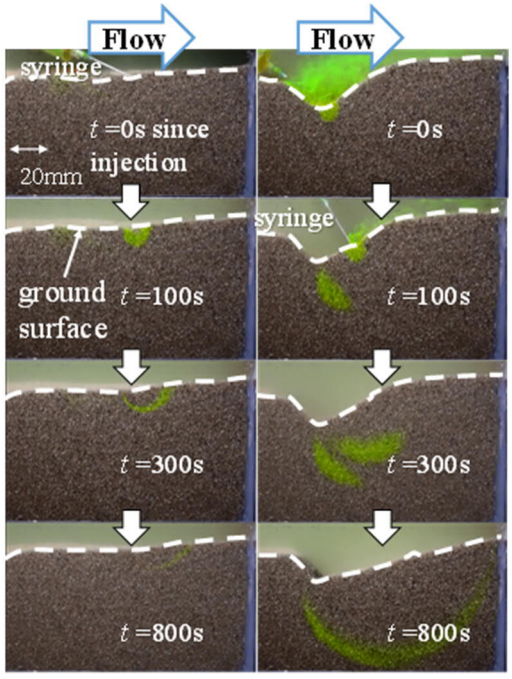

Figure 9. Seepage trajectories from valleys of ripples by observation method (B): silica sand #5; v_{ave} = 0.31 m/s

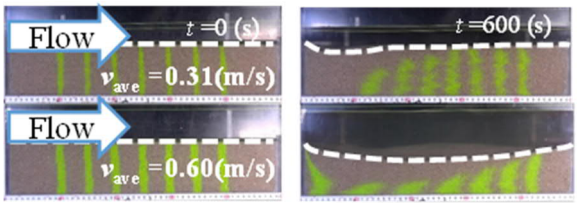

Figure 10. Seepage behaviors in ground by observation method (C): silica sand #5.

Figure 11 shows the depth distribution of the excess pore water pressure u_e when the relative positions of the pore water pressure sensor (p.w.p.s. in the figure) and the ripple seepage region on the ground surface were different. The excess pore water pressure was negative near the seepage flow entry in the left figure, supporting the inflow, whereas the excess pore water pressure was positive near the exit of the seepage flow in the right figure. Based on soil engineering, the former increases the effective stress of the soil and stabilizes, whereas the latter decreases it and destabilizes the soil, resulting in liquefaction when the flow velocity is high. In other words, seepage induced by the horizontal flow and riverbed waves change the stability of the soil and is thought to have a major effect on the scouring process.

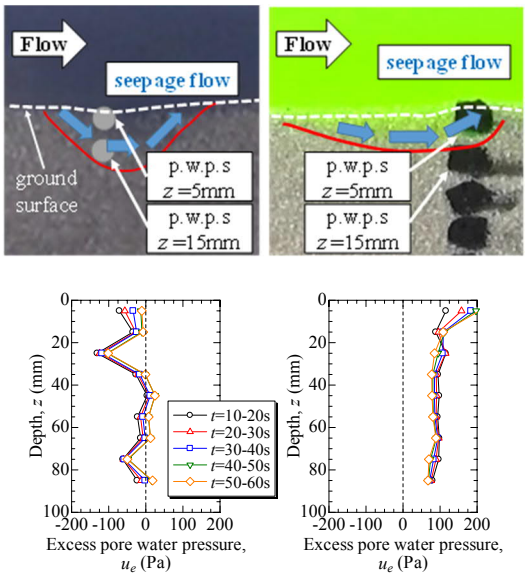

Figure 11. Seepage directions and behaviors and excess pore water pressure: photos at t = 55 s.

4 CONCLUSIONS

In this study, model experiments for a water channel with a mobile seabed and visualization experiments of seepage into the ground, which were thought to be one of the causes of excess pore water pressure occurring in the ground during high-speed fluid action, were performed to examine the seepage behavior of fluid into the ground.

The seepage had an arc wave shape and was thought to enter from the riverbed wave valleys and flow out from the ground near the peaks. This seepage flow action moved pore water in the ground and generated excess pore water pressure not only in the ground surface layer but also at the depths. Moreover, the seepage region may become larger in proportion to the wave height magnitude of the riverbed waves in a tractive flow state. The pressure differences in the cross-sectional flow velocity due to the riverbed wave formed during fluid action helped display the seepage behavior. As a result, new ground micromechanics for scouring were constructed.

5 REFERENCES

Matsuda, T., Maeda, K., Izumi, N., Ito, Y., Yamaguchi, A., Tsurugasaki, K., and Miyamoto, J. 2016. A Consideration on the generating mechanics of excess pore water pressure in the sandy ground induced by surface flow (in Japanese), Journal of JSCE, Ser. B2, Coastal Engineering (in Japanese), 72(2), I_565–I_570.

Matsuda T., Maeda, K., Miyake, M., Miyamoto, J., Sumida, H. and Tsurugasaki, K. 2016. Instability of a caisson-type breakwater induced by an earthquake–tsunami event, International Journal of Geomechanics, ASCE, 16(5), C4016003-1-10.

Suzuki, Y., Maeda, K., Matsuda, T. and Takagi, K. 2016. Factor analysis for generating excess pore water pressure due to seepage caused by horizontal flow, Journal of JSCE, Ser. B2, Coastal Engineering (in Japanese), 74(2), I_721–I_726.